ACS central science

http://pubs.acs.org/journal/acscii

Outlook

Metal@Zeolite Hybrid Materials for Catalysis

Hai Wang, Liang Wang,* and Feng-Shou Xiao*

Cite This: *ACS Cent. Sci.* 2020, 6, 1685−1697

Read Online

ACCESS | Metrics & More | Article Recommendations

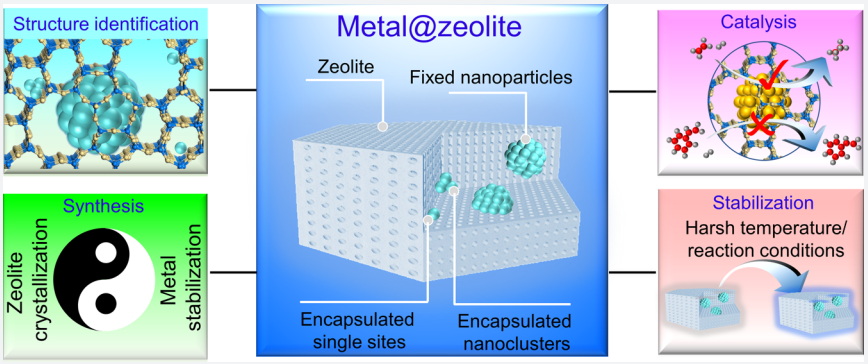

ABSTRACT: The fixation of metal nanoparticles into zeolite crystals has emerged as a new series of heterogeneous catalysts, giving performances that steadily outperform the generally supported catalysts in many important reactions. In this outlook, we define different noble metal-in-zeolite structures (metal@zeolite) according to the size of the nanoparticles and their relative location to the micropores. The metal species within the micropores and those larger than the micropores are denoted as encapsulated and fixed structures, respectively. The development in the strategies for the construction of metal@zeolite hybrid materials is briefly summarized in this work, where the rational preparation and improved thermal stability of the metal nanostructures are particularly mentioned. More importantly, these metal@zeolite hybrid materials as catalysts exhibit excellent shape selectivity. Finally, we review the current challenges and future perspectives for these metal@zeolite catalysts.

INTRODUCTION

The catalytic performances of heterogeneous catalysts can be adjusted by the catalyst structures.[1−13] In this respect, it is highly desired to develop unique catalyst structures with proof-in-concept designs for the target reactions. Compared with the metal nanoparticles generally supported on the external surface of solid supports, localizing them within a confined species usually leads to improvements in the catalytic performances.[14−21] Successes have been achieved in encapsulating metal nanoparticles within carbon nanotubes, which improves the surface charge and enhances the catalytic activity of Fe nanoparticles in Fischer−Tropsch (F-T) synthesis,[15] RhMn nanoparticles in the syngas-to-ethanol transformation,[22] and Cu nanoparticles in the ester hydrogenation.[23] Comparing carbon nanotubes with an electronic effect to the metal nanoparticles, the mesoporous silica is electronic-inert but it also contributes to the metal nanoparticle stabilization by encapsulation within the mesoporous channels.[19,24,25] In addition to these mesoporous materials with metal nanoparticles, they are expected to combine the metal nanoparticles with the porous materials with smaller pores, such as micropores with sizes at a single molecule level.

Zeolite is a solid material with a well-defined microporous structure, uniform acidic/basic sites, and good thermal/hydrothermal stability.[26−29] Owing to these features, zeolite supported metal nanoparticles have already been used in many important industrial processes, such as catalytic isomerization, cracking, and hydrogenation reactions.[30−34] In these cases, the metal nanoparticles are mostly loaded on the external surface of zeolite crystals, which might proceed the migration and Ostwald ripening[1,2,35−37] that cause metal sintering to lose the activity. In order to overcome this problem, it has been developed to introduce metal species into the zeolite crystals, obtaining a series of unique catalysts denoted as metal@zeolite catalysts.[38−42] These catalysts exhibit improved metal sinter resistance compared with the supported nanoparticles because of the stabilization of these metal nanoparticles by the rigid zeolite framework. In addition, shape-selective catalysis, an

Received: August 23, 2020
Published: September 25, 2020

https://dx.doi.org/10.1021/acscentsci.0c01130
ACS Cent. Sci. 2020, 6, 1685−1697

important feature of zeolite catalysts, is also introduced in these metal@zeolite catalysts.[38,42,43] This is another advantage of metal@zeolite structure that is rarely achieved on the supported metal nanoparticles. In this case, the zeolite micropores act as the channels for the molecular diffusion and reaction, which bring a new opportunity to adjust the reaction process by engineering the zeolite micropores.

The aforementioned advantages of metal@zeolite catalysts motivated the investigation of the synthesis of these hybrid materials. In the beginning, the introduction of metal species in zeolite micropores is performed from metal cation exchange in the liquid phase or metal migration at a high temperature.[44−49] Later, it is employed *in situ* synthesis for introduction of metal nanostructures within the zeolite crystals. Generally, the metal precursors are directly added into the zeolite crystallization gel. In this case, many metal species favor the formation of depositions in the gel because of the high surface free energy of metal species, strong alkalinity of the hydrothermal system, and relatively high temperature of the zeolite crystallization.[50−55] This is to say, the stabilization of metal precursors to avoid leaching, agglomerating, and precipitating is crucial for obtaining the ideal metal@zeolite structure.[39,56−58] Following this knowledge, the organic ligands are used to reduce the surface free energy of the metal species and stabilize them under crystallization conditions. With regard to green synthesis without using the organic ligand and/or improving the capsulation efficacy, a series of different methodologies were developed. Typically, the solvent-free route minimizes the metal leaching and agglomeration in the solid-state crystallization;[59−61] the metal-containing-seed-directed route constructs the core−shell structure without using any organic species,[62] where the zeolite seeds help to stabilize the metal nanoparticles. The fast crystallization method balances the rates of metal precipitation and zeolite crystallization, which forms the zeolite framework before metal precipitating.[63] In addition to the development in synthesis methodologies, the metal@zeolite catalysts exhibit improved performances compared with the generally supported catalysts.

With the significant advantages and increasing achievements for metal@zeolite catalysts, there have been several reviews focusing on this topic.[38,64] This Outlook does not repeat the details that have been already summarized in the previous reviews, but will briefly show the concepts in metal@zeolite catalysts and overview the developing trend in synthesis strategies, where the rational preparation for constructing the desired structures is particularly discussed. As well, the advantages of metal@zeolite materials in catalysis are mentioned. In addition to these contents, we also review the current challenges and future perspectives for these metal@zeolite catalysts.

CLASSIFICATION OF METAL@ZEOLITE STRUCTURES

Metal species with different diameters could be formed within the zeolite crystals, including isolated metal sites, nanoclusters, and nanoparticles. The isolated metal sites and small nanoclusters are well-defined within the zeolite micropores/cages, where the metals are usually moveable in the microporous channels under harsh conditions. This is denoted as the encapsulated structure (metal sizes are smaller than the micropore/cage sizes). Besides, it is also developed to form metal nanoparticles, which are larger than the micropores, into the zeolite crystals. In order to distinguish them from the metal clusters within the micropores, we denoted them as fixed structures (metal sizes are obviously larger than the micropore/cage sizes). The isolated metal sites/nanoclusters encapsulated and nanoparticles fixed in zeolite crystals are shown in Figure 1.

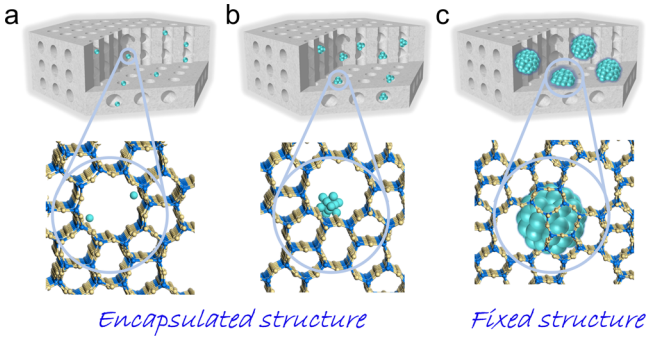

Figure 1. Metal@zeolite with encapsulated and fixed structures. (a) Isolated metal sites and (b) metal nanoclusters encapsulated in the micropores. (c) Metal nanoparticles fixed in the zeolite crystals.

ZEOLITE ENCAPSULATED SINGLE METAL SITES

Owing to the electronically negative aluminosilicate framework, "guest cations", such as Na^+, exist in the micropores to make the electrically neutral. As these cations are fairly mobile and easily exchanged, the metal cations could be introduced into the zeolites by exchanging with Na^+.[44−46,65−68] Following this feature, a wide scope of metal-based catalysts have been developed by inducing various cations into the zeolite, such as the Cu-Y, La-Beta, Zn-ZSM-5, and many others.[67−79] In addition, noble metal cations could be also exchanged into the zeolite for the site-isolated catalyst with a well-defined structure, such as the $[Pt(NH_3)_4]^{2+}$ and $Ir(C_2H_4)_2^+$ exchanged within K-LTL and H/Na-Y zeolites (Figure 2a−e).[80,81] Removing the ammonia ligand of $[Pt(NH_3)_4]^{2+}$ in LTL maintains the isolated Pt sites that bonded to the oxygen on the zeolite framework,[80] but the Pt location differs from the original $[Pt(NH_3)_4]^{2+}$ in LTL. In detail, most of the $[Pt(NH_3)_4]^{2+}$ complexes are observed initially in the large pore of LTL zeolite (Figures 2f−l). After the oxidation treatment, part of the Pt atoms in the large pores are moved from the large pores into smaller pores, which reveals the mobility of isolated atoms within the zeolite micropores.

The ion-exchange in aqueous solution does not work for the cations with a high valence state (e.g., M^{3+}), because of the high energy barrier for simultaneously exchanging three positive charges (e.g., K^+, Na^+) in the zeolite micropores. Solid-state dispersed metal sites in the micropores at high temperature (500−550 °C) could overcome this limitation. For example, a series of specific operations, including impregnating, calcining, and reducing with H_2, to the $Rh(NO_3)_3$ species on ZSM-5 surface, could result in single-site Rh within the zeolite micropores.[82] The single-site Rh is shown as Rh^+ because of the bonding with the oxygen species.

In addition, the post-treatment method might disperse the noble metal atoms on the shallow layers of zeolite crystals. *In-situ* encapsulation, a concept that is realized by inducing the atomically dispersed metals within zeolite during the crystallization, would benefit the uniform metal distribution through the zeolite crystals. However, direct addition of the metal salts into the zeolite crystallization system usually forms

https://dx.doi.org/10.1021/acscentsci.0c01130
ACS Cent. Sci. 2020, 6, 1685−1697

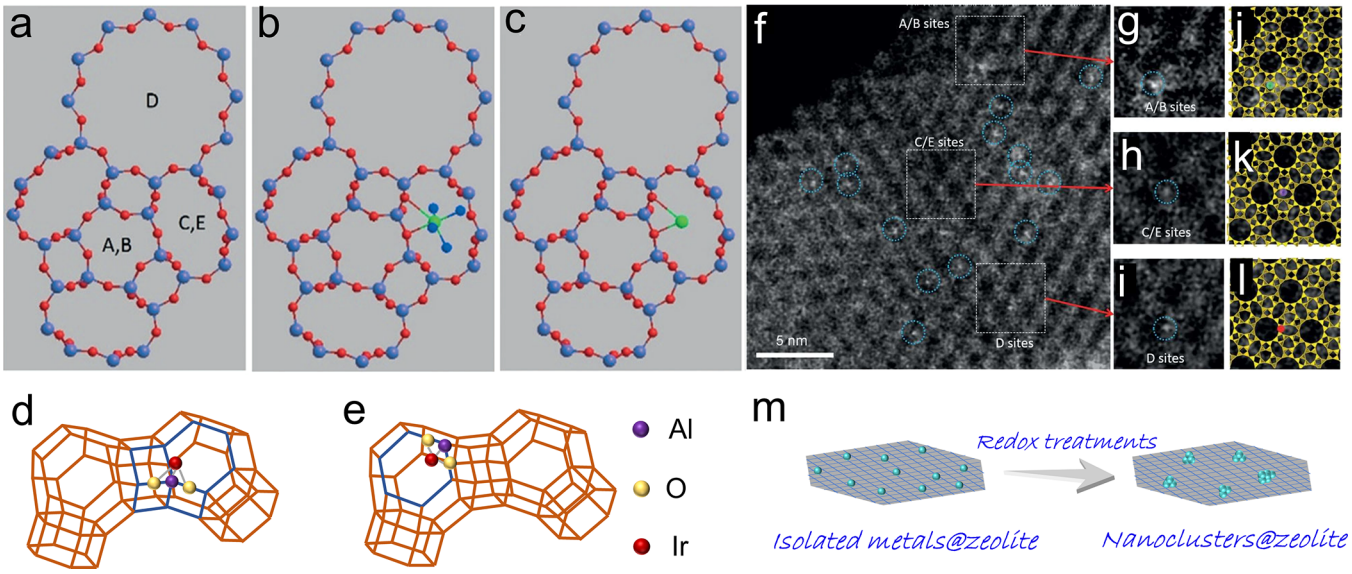

Figure 2. (a–c) Models of zeolite LTL with (a) different pore and (b) $[Pt(NH_3)_4]^{2+}$ and (c) PtO_x located in the 8-MR. Reprinted with permission from ref 80. Copyright 2014 Wiley-VCH. The models illustrate the positions of the Ir^+ ions: (d) T5, three-hollow position, (e) T6, six-ring. (f) STEM images showing site-isolated Pt atoms in KLTL zeolite in the as-prepared samples. White features in dashed blue circles indicate Pt atoms. (g–i) Magnified views of the highlighted regions in (f), containing one Pt atom each at A/B sites in (g), at C/E sites in (h), and at D sites in (i). (j–l) Simulations of the LTL zeolite in the [110] direction superimposed on the magnified views in (g–i), showing Pt atoms (green) at A/B sites in (j), at C/E sites in (k) (purple), and at D sites in (l) (red). Pt atoms are located right at the edge of the 12-membered rings of site D; between the two 12-membered rings of sites C/E; and in the center of three 12-membered rings of sites A/B. Reprinted with permission from ref 80. Copyright 2014 Wiley-VCH. (m) Schematic illustration of the aggregation of Pt species during the redox treatment.

As a principle to guide the successful synthesis of metal@zeolite, it is required to stabilize the metal species and enhance the interactions between metal-precursor and zeolite units.

the separated phases of both zeolite crystals and metal (hydroxide) precipitates, which is due to the extremely fast metal agglomeration and precipitation under the zeolite synthesis conditions (strong alkalinity and high temperature)[50−55] because of the high surface energy. Generally, the metal salts are transformed into bulky species before the zeolite crystallization. Therefore, the interactions between the metal species and the zeolite precursors/building units is a key for the formation of the encapsulated structure.

Success is achieved by using organic ligands, which strongly coordinate with the metal species to reduce the free energy. As well, the solvated metal−ligand complex with alkaline ligands also benefit the assembly of the zeolite building units around such species by electrostatic or van der Waals interactions. The isolated Pt sites in NaY zeolite could be prepared by adding the complex of ethylenediamine-Pt cations into the zeolite crystallization system.[83] Because the coordination of ethanediamine to Pt cations is stronger than OH^-, the Pt is atomically dispersed throughout the crystallization process with switched off metal precipitation and agglomeration. Such synthesis strategy could also be extended to the other metals, including the Pd, Ru, Rh, Co, Ni, and Cu,[83] which ideally obtained the metal species uniformly distributed in the FAU zeolite crystals. The pore size and structure of FAU zeolite make a significant contribution to the high dispersion of the metal-ethanediamine complex because each nanosized β-cage can ensconce only one metal-ethanediamine and constrain it by the small windows. This strategy has similarity with the fish-in-bottle concept that has guided the isolation of transition metal sites in zeolite by post treatment using the ligand−metal complex with appropriate diameters.[84]

The encapsulation of isolated metal sites within the siliceous zeolite crystals seems more challenging because of the neutral zeolite framework and harsh crystallization conditions (higher temperatures and stronger alkalinity), compared with the synthesis of FAU zeolite. In addition, the siliceous zeolite is usually synthesized in the presence of the organic template, and removal of these organic templates by calcination generally results in aggregation of the metal atoms into clusters or even larger particles in the air. With this issue, a direct hydrogenation could simultaneously remove the organic template and maintain the atomically dispersed metals in the zeolite crystals.[57] On the basis of these examples, we conclude that the organic ligands, metal loadings, and post-treatment methods are crucial for obtaining atomically dispersed metals within zeolite micropores.

These atomically dispersed metals in zeolite are movable, which possibly leads to the agglomeration from single atoms into metal nanoclusters under the redox treatments (Figure 2m).[80,85] However, surprising stability of Rh sites is observed in the siliceous MFI zeolite; the atomic dispersion is well maintained at even 700 °C in hydrogen.[57] This phenomenon is explained by the location of Rh sites in the 5-MR (membered ring) of the MFI structure, which hinders the mobility of metal nanoparticles,[57] while the larger pores, such as 8- and 10-MR, allow the diffusion of metal atoms that would agglomerate under harsh conditions.[57,85]

https://dx.doi.org/10.1021/acscentsci.0c01130
ACS Cent. Sci. 2020, 6, 1685−1697

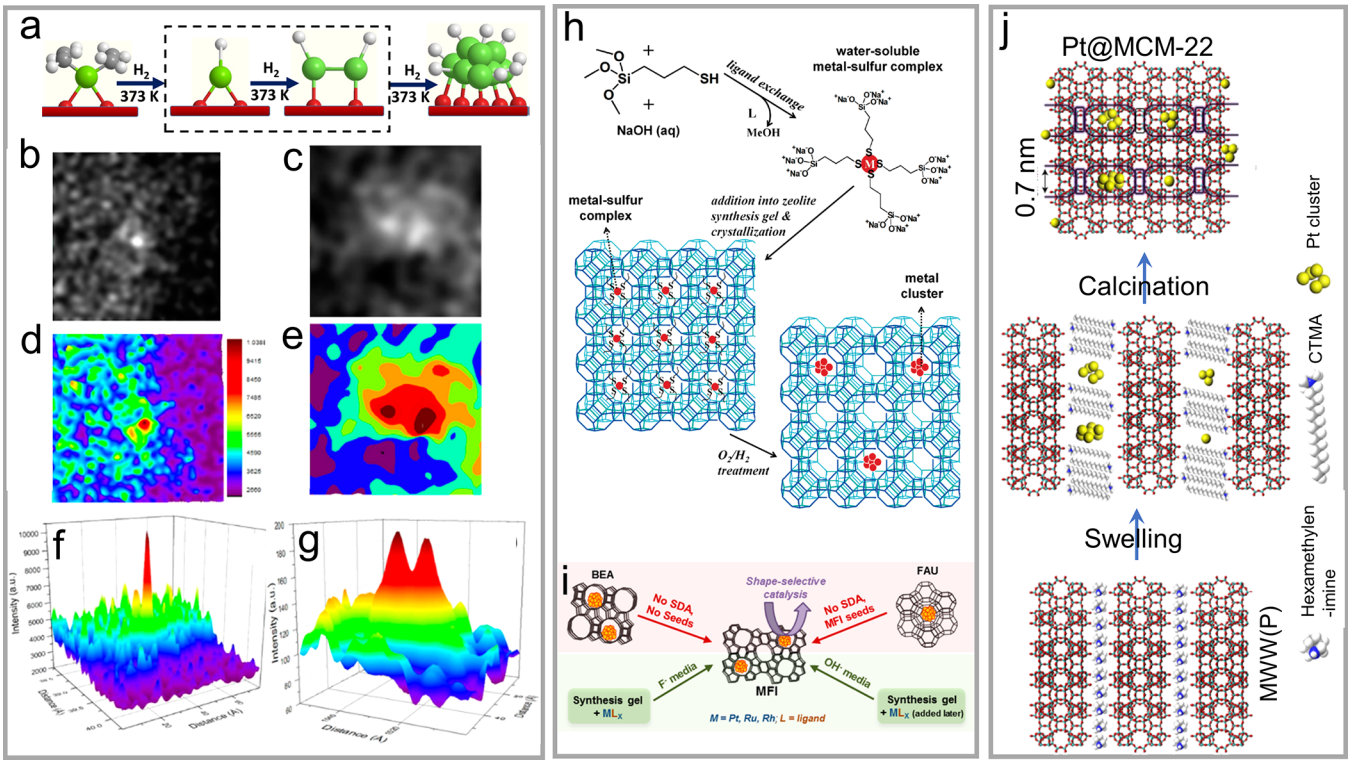

Figure 3. (a) Scheme showing the transformation of single-site Rh into Rh_2 clusters. Magnified view of the (b) Rh atom and (c) Rh_2 cluster in the HAADF-STEM image with (d, e) intensity surface plot and (f, g) three-dimensional intensity surface plot. Reprinted with permission from ref 86. Copyright 2016 American Chemical Society. (h) Metal@zeolite synthesis using bifunctional ligand of (3-mercaptopropyl)trimethoxysilane. Reprinted with permission from ref 39. Copyright 2010 American Chemical Society. (i) Interzeolite transformation route and conventional hydrothermal synthesis route for preparing metal@zeolite materials. Reprinted with permission from ref 40. Copyright 2014 American Chemical Society. (j) Preparation of Pt@MWW by inducing Pt species during the swelling process of layered zeolite precursors. Reprinted with permission from ref 91. Copyright 2017 Nature Publishing Group.

ZEOLITE ENCAPSULATED METAL NANOCLUSTERS

The migration and agglomeration of metal atoms in the micropores effectively give rise to the formation of encapsulated nanoclusters. This transformation process was identified by employing a model of ethene-stabilized Rh in HY in hydrogen atmosphere.[86] The ethene ligands on the Rh atoms react with hydrogen to form Rh hydrides (RhH_x), which is regarded as a crucial intermediate for the Rh atom migration and aggregation. Rh_2 clusters, the smallest Rh nanoclusters containing two Rh atoms, are formed in the beginning of the Rh atom agglomeration (Figure 3a–g).

Similar to a developing trend of atomically dispersed metal in zeolite, it is highly desired to *in situ* encapsulate the metal nanoclusters, which involves introducing cationic complex into the zeolite synthesis gel and then assembling the zeolite building units around such species. The RuO_2 nanoclusters were encapsulated within FAU zeolite using $RuCl_3$ or $Ru(NH_3)_6Cl_3$ as the precursors.[50] Zeolite confined the growth of the RuO_2 cluster, as revealed by the cluster size at 1.3 nm that is comparable to the super cage of FAU zeolite. In this case, $RuCl_3$ or $Ru(NH_3)_6Cl_3$ were directly used as the precursors without an additional organic ligand, where the Cl^- and NH_3 should help stabilize the metal sites during the zeolite crystallization. However, they only work for limited metals (e.g., Ru), and the organic ligand is usually needed for encapsulating different metals.

The bifunctional organic ligands could simultaneously stabilize the metal precursors and interact with zeolite building units. A typical molecule is (3-mercaptopropyl)-trimethoxysilane that condensates with the silicate zeolite structures and coordinates to the metal sites during the zeolite crystallization (Figure 3h).[39] Because of the strong coordination of the mercapto group, metal agglomeration and precipitation were hindered under the hydrothermal zeolite crystallization system. The alkoxysilane group of the metal–ligand complex undergoes hydrolysis and formation of Si–O–Si or Si–O–Al bonds to the zeolite structures, thus driving the zeolite formation around the metal species to form an encapsulated structure. The Pt, Pd, Ir, Rh, and Ag nanoclusters were also synthesized within the cages of NaA zeolite using the bifunctional ligands.

As mentioned above, the ethylenediamine ligands coordinated with metal cations are stable under the alkaline conditions, which also effectively interact and couple with the Si and Al species that are crystallized into the zeolite framework. Following the operation in preparing zeolite encapsulated single site metals, raising the metal loading could efficiently obtain the zeolite encapsulated metal nanoclusters. Successes were achieved in the preparation of MFI zeolite encapsulated Pd,[52] Pt,[58] PdNi,[55] PtZn,[58] PtSn,[17] and PdMn[87] nanoclusters by the direct use of ethylenediamine coordinated multiple metal species in the zeolite crystallization system. Even for small-micropore zeolite (6-MR), such as SOD, GIS, and ANA, the ethylenediamine ligand still works well for the formation of small nanoclusters within the zeolite

https://dx.doi.org/10.1021/acscentsci.0c01130
ACS Cent. Sci. 2020, 6, 1685–1697

crystals.[56] In sum, ligands with bifunctions including coordination with the metal sites, and electrostatic or van der Waals interactions with the zeolite precursors/units, link the metal and zeolite species to form the desired metal@zeolite structure.

The encapsulation of metal nanoclusters was also realized by the interzeolite transformation, where the organic ligands are not necessary. The metal cations were exchanged into a parent zeolite and reduced into metal nanoclusters, followed by the crystal transformation into another type of zeolite. In the study by Goel et al., the BEA and FAU zeolite with low framework density were employed as the parent zeolite, and the transformation occurred under the assistance of MFI seeds or organic templates (Figure 3i).[40] An attractive observation is that the nanoclusters on the parent zeolites are unchanged in sizes on the final samples, which reveals the stabilization effect of zeolite species to the metal nanoparticle. Possibly, the zeolite framework building units and/or small crystals grow around the metal clusters, thus to hinder the metal sintering. The successes in encapsulation of Pt, Ru, and Rh nanoparticles into the MFI zeolite fairly confirm the university of this method on different metal species. Notably, the interzeolite transformation only occurred from the low-density zeolites (e.g., Beta and Y) to high-density ones (e.g., ZSM-5).[40,88,89]

We emphasize that the isolated metal sites and metal nanoclusters are reversibly transformed within the zeolite micropores under the different treatments. The Pt nanoparticles, with sizes at about 1 nm and encapsulated within the siliceous CHA zeolite, were redispersed as isolated Pt sites under the oxidation treatment, while the reduction leads to the reverse into Pt nanoparticles at 1 nm.[90] Notably, the conventional reversible transformation of metal nanoclusters and the isolated metal sites usually occur under the very mild temperatures (<80 °C) to avoid irreversible formation of large particles upon sintering. Interestingly, in the siliceous CHA zeolite, the redox treatment could be performed as the temperatures as high as 650 °C, confirming the superior sinter resistance. In the transformation of isolated Pt atoms into nanoclusters under the reduction treatment, it is proposed that the Pt atoms, which are localized within the different cages of zeolite, might migrate in hydrogen through the 8-MR windows to form nanoclusters within the CHA micropores/cages.

Notably, for the redox treatment of metal@zeolite materials, the metal atom migration to the external surface of zeolite is energy-unfavorable because of the long migration distances and easy formation of nanoclusters from the atoms nearby. In the oxidative treatment, the Pt migration might occur in the PtO form, which is well demonstrated in the Pt migration mechanism. Possibly, the zeolite framework should have strong interactions with the isolated Pt sites via SiO- or AlO-linkage, because the Pt atoms are too small to be physically confined within the 8-MR rings.

Liu et al. introduced the Pt species within the zeolite crystals during the transformation of two-dimensional zeolite into three dimensions.[91] As shown in Figure 3j, purely siliceous MWW zeolite (ITQ-1) was used as the matrix, and the Pt species, that are subnanometric Pt in dimethylformamide, were introduced during the swelling process of layer MWW. In this process, the subnanometric Pt and the surfactant molecules (molecules to swell the zeolite) were localized between the layers. After calcination to remove the organic species, the Pt nanoclusters were formed and encapsulated between the supercages of MWW zeolite. In addition, some Pt species were also confined in the cups located at the external surface of the zeolite crystals.

With regard to the stability issue, the Pt nanoclusters in the MWW zeolite slightly aggregate into larger ones with sizes at 1−2 nm after the oxidation−reduction treatments for 1 cycle at a harsh temperature of 650 °C. The clusters at such diameters should be captured by the supercages of MCM-22 zeolite. With the continuous redox treatments for several cycles, the atomically dispersed Pt and ultrasmall clusters are almost undetectable, but the Pt nanoclusters are mostly below 2 nm. Undoubtedly, the stability originates from the encapsulated structure, and the Pt nanoclusters supported on the external surface of MWW zeolite easily sintered into large particles.

In addition, we have to note that the Pt@MCM-22 catalyst still suffers from Pt leaching and sintering during the catalysis or treatment under harsh conditions because of the lower metaling and boiling point of Pt nanoclusters,[92−94] even if Pt@MCM-22 has improved stability compared with the generally supported Pt. For example, after continuously redox treatments (four cycle reduction−oxidation at 650 °C), the Pt@MCM-22 has only 30% of the initial Pt, because the mobility of the Pt clusters in the zeolite micropores led to the metal loss.

■ ZEOLITE FIXED METAL NANOPARTICLES

With the aforementioned stability issues, it is expected to further stabilize the metal nanostructure by hindering the metal mobility in the zeolite crystals. To achieve this goal, fixation of the metal nanoparticles by the zeolite framework is desired rather than encapsulation of them in the micropores. On the other hand, most of the industrial supported metal nanoparticle catalysts have diameters in the range of several nanometers (e.g., 1.5−4.0 nm),[95−97] which are obviously larger than the micropores. This knowledge also motivated the study in fixing the metal nanoparticles with desirable diameters in the industrial range.[43,62,98]

In the synthesis of zeolite fixed metal nanoparticles, the stabilization of metal precursors under the zeolite crystallization system and interactions between the metal precursors to the zeolite building units are still crucial factors. Different from the synthesis strategies in zeolite encapsulated metal nanoparticle catalysts, where the metal nanoclusters are formed during or after the zeolite crystallization, the metal nanoparticles with desired diameters should be formed before the zeolite framework formation, which avoids the encapsulation of metal species in the micropores. For achieving the fixation of metal nanoparticles with zeolite crystals, a typical route is the controllable hydrolysis of the tetraethyl orthosilicate to form an amorphous silica sheath around the metal nanoparticles (e.g., Au). Then, the amorphous silica species are crystallized into S-1 zeolite under hydrothermal conditions with the assistance of the tetrapropylammonium hydroxide template.[42] The Au nanoparticles are partially fixed within the zeolite crystals, but there are still Au nanoparticles on the zeolite external surface. In the calcination treatment, the Au nanoparticles in the zeolite crystals were efficiently stabilized even under the harsh temperature, but those on the external surface easily sintered into larger particles. In addition, the Au species might leach and agglomerate during the AuPd@S-1 growth, because of the amorphous silica dissolution in the liquor under hydrothermal conditions. This feature results in low Au utilization efficacy (percentage of Au species in the final product to that in the starting solution), which could be improved by the solvent-free synthesis.[99,100] If the amorphous

https://dx.doi.org/10.1021/acscentsci.0c01130
ACS Cent. Sci. 2020, 6, 1685−1697

silica fixed metal nanoparticles (e.g., AuPd) are crystallized in the solid state without adding solvent, higher than 96% AuPd species would be obtained into the final AuPd@S-1 sample. In contrast, metal utilization is only 34−36% by a conventional hydrothermal route.[59]

The metal nanoparticles are usually larger than 5 nm in the above cases, because PVP has a limited ability to stabilize the metal nanoparticles. A new method, which is denoted as metal-containing-seed-directed zeolite crystallization, could overcome the limitation in nanoparticle size control in the metal@zeolite structure.[62] This synthesis is realized by loading metal nanoparticles on the zeolite crystals, obtaining the metal/zeolite seeds, which were used for the synthesis of new zeolite crystals (Figure 4a). Because the seed-directed zeolite

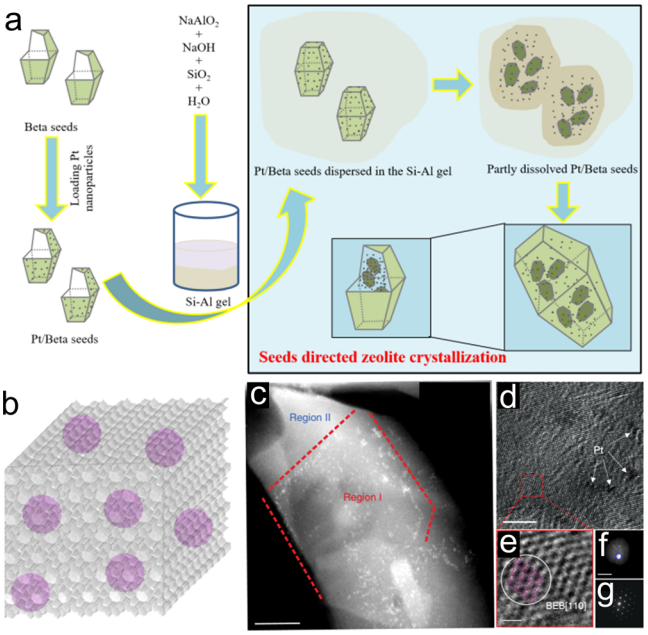

Figure 4. (a) Proposed growth mechanism of metal nanoparticles fixed in zeolite crystals. (b) Model of metal@zeolite hybrid materials. (c−g) TEM characterization of Pt@Beta. (c) STEM image characterizing the platinum nanoparticle distribution. Region I might be the zeolite seed with abundant Pt species, and region II should be the newly formed zeolite with negligible Pt. The dashed line shows the boundary of Region I. (d) HR-TEM image of Pt@Beta. (e) Enlarged view of the red square in (d). The white circle highlights the microdomains of polymorph B (BEB) of zeolite Beta, overlaid by a BEB structure model viewed along [110]. (f) STEM image of a Pt@Beta sample crystallized at 4 h. (g) Corresponding electron diffraction pattern of the circle in (d). Scale bars: 50 nm in (c), 20 nm in (d), 25 Å in (e), and 500 nm in (f). Reprinted with permission from ref 62. Copyright 2018 Nature Publishing Group.

crystallization follows a core−shell mechanism, smaller seed crystals with metal nanoparticles, which are formed from partial dissociation of the seed crystals, are fixed by the silica precursors in the beginning of the crystallization, thus to isolate the metal nanoparticles to avoid agglomeration. Finally, the amorphous aluminosilicate sheath was transformed into the zeolite framework, thus to fix them within the zeolite crystals (Figure 4b). This method is universal for the synthesis of different metal nanoparticles fixed within the zeolite crystals, giving the Pt, Ag, Pd, and Rh nanoparticles in Beta, MOR, and S-1 zeolites.

In the seed-directed route for metal@zeolite synthesis, the metal nanoparticles before and after the zeolite crystallization are unchanged because of the strong interactions between the zeolite seeds and metal nanoparticles, as well as the fixation effect from the amorphous aluminosilicate and zeolite building units (Figure 4c−g). Owing to this advantage, the metal nanoparticles in the metal@zeolite samples could be effectively controlled by adjusting their sizes on the seeds. By using this technique, the Pt@Beta samples containing Pt nanoparticles with a diameter range at 0.8−3.2, 1.2−3.6, and 1.6−6.0 nm are obtained. In addition to the controllable metal nanoparticle diameters, a significant advantage of the seed-directed route is the avoidance of any organic species in the synthetic process. Because of the bifunctions of zeolite seeds including the stabilization of metal nanoparticles and direction of zeolite growth, the organic ligand and template were not employed, which has been regarded as a green synthesis route.

On the basis of the aforementioned discussion, the developing trend in metal@zeolite synthesis is from the random growth to the controllable assembly, from the costly process to the green route (Figure 5). Having better control of the diameter of metal nanoclusters/particles and their encapsulation/fixation within the zeolite crystals is highly desired. In order to achieve this goal, rationally controlling the interaction and assembly of metal species and zeolite precursors/building units is important. The organic ligands have worked effectively in bridging the metal and zeolite, but new synthetic methods, such as the seed-directed route, exhibit great potential for controllable synthesis even with abandoning the organic ligands.

CATALYSIS BY METAL@ZEOLITE

The metal@zeolite catalysts have been extensively studied in various reactions, including oxidation,[42,59,74−76,82,101,102] hydrogenation,[57,60,61,103] reforming,[52,55,62] and coupling.[38] Compared with the generally supported metal nanoparticle catalysts, two of the most significant advantages of metal@zeolite catalysts are sinter resistance of metal nanoparticles and shape selectivity in metal-catalyzed reactions.

SINTERING- AND LEACHING-RESISTANT CATALYSTS

The zeolite fixed metal nanoparticle catalysts are extremely stable in various reactions for the transformation of C_1 molecules, including the water−gas shift, CO oxidation, oxidative reforming of methane, and CO_2 hydrogenation.[62] In both catalysis and regeneration under redox conditions at a high temperature, metal nanoparticle sintering and metal loss are unobservable. This feature is due to the difficult motion of metal nanoparticles fixed by the zeolite framework, which is also the most important difference with the encapsulated metals in the micropores.

Noble metal leaching usually occurs to cause the deactivation. For example, the Pd leaching is a general problem for many supported Pd nanoparticle catalysts, which is also a serious problem faced by Pd catalyst industries. For example, in the hydrogenation of 4-nitrochlorobenzene, 6.7% of Pd species on commercial Pd/C catalyst was leached in the reaction for 90 h, which is accompanied by a significant loss of activity.[103] Very interestingly, the Beta zeolite fixed Pd nanoparticles exhibited unchanged catalytic activity with negligible Pd leaching under the equivalent reaction con-

https://dx.doi.org/10.1021/acscentsci.0c01130
ACS Cent. Sci. 2020, 6, 1685−1697

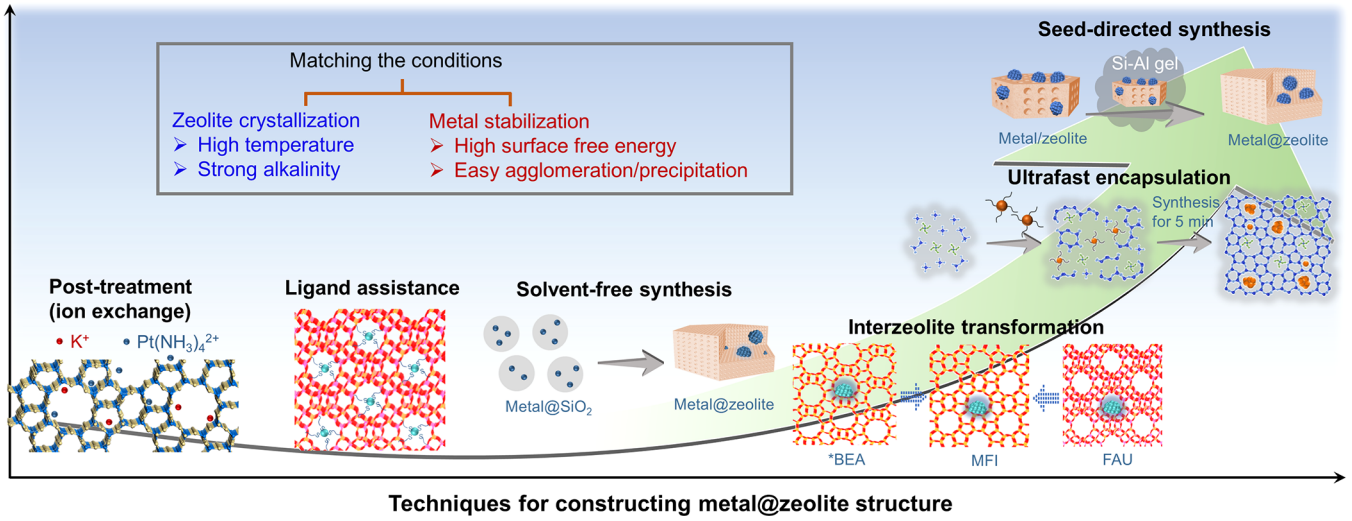

Figure 5. Techniques for constructing a metal@zeolite structure. Models in the ultrafast encapsulation technique are reprinted with permission from ref 63. Copyright 2020 Wiley-VCH.

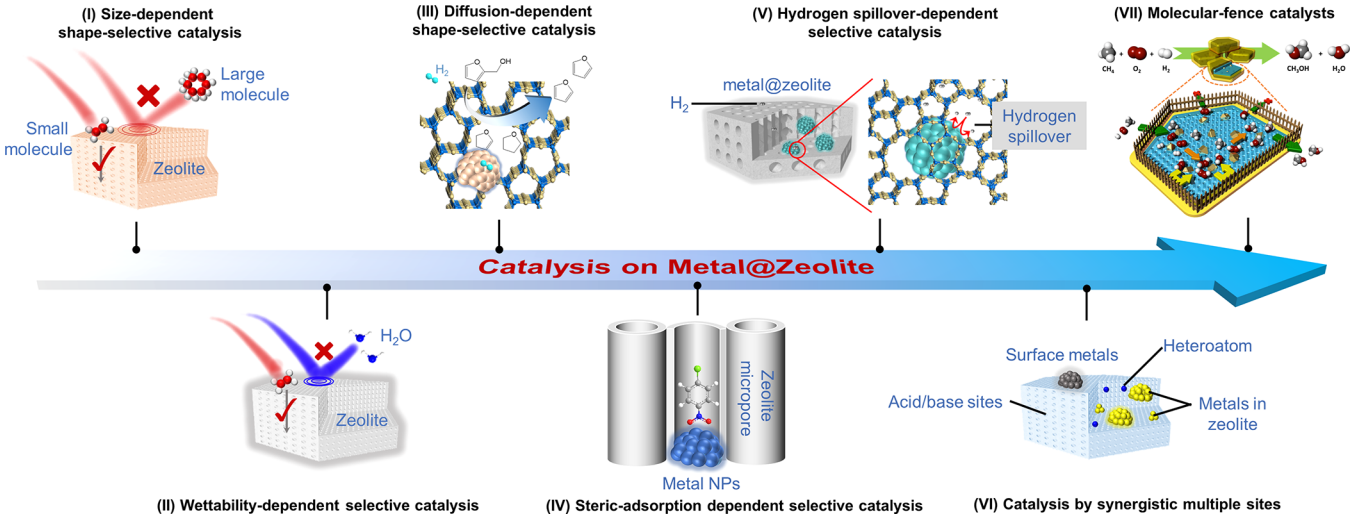

Figure 6. Catalysis on metal@zeolite hybrid materials.

ditions.[103] The leaching resistance of zeolite fixed Pd nanoparticles was also confirmed in the Suzuki cross coupling reactions, where the Pd@S-1 exhibited constant activity in the recycle tests for 15 runs.[104]

SIZE-DEPENDENT SHAPE-SELECTIVE CATALYSIS

Zeolite micropores could sieve the molecules during the catalysis, thus introducing shape selectivity to the metal catalyzed reactions. Because the metal nanoparticles are localized within the zeolite crystals, the zeolite micropores could selectively allow the diffusion of molecules with diameters smaller than the micropores and hinder the access of bulky molecules to the metal species, known as size-dependent shape selectivity (Figure 6I). For example, in the Suzuki cross coupling reactions with different substrates, Pd@S-1 is active for the coupling of small molecules, while the molecules containing multiple functionalized groups with larger sizes failed to be converted because of the micropore size limitation.[104] In the hydrogenation of multiple olefins with distinguishable diameters (e.g., ethene and cyclohexene), the metal@zeolite could selective catalyze the conversion of olefins smaller than the micropore sizes.

WETTABILITY-DEPENDENT SELECTIVE CATALYSIS

The supported Au nanoparticles have been extensively studied in the ethanol oxidation, which usually leads to the sintering of Au nanoparticles and deactivation.[105−108] The S-1 fixed Au nanoparticles, denoted as Au@S-1, exhibited stable performances in a continuous reaction for a long time.[42,107] With regard to the oxidation of bioethanol, it contains abundant water that hinders the reaction by water−ethanol competitive adsorption on the metal surface. The siliceous zeolite fixed catalyst could minimize the influence of water to the reaction by a wettability-dependent selective feature (Figure 6II): the hydrophobic siliceous zeolite hinders the water transfer and benefits ethanol transfer, realizing the ethanol−water separation from each other on the local environment close to the metal nanoparticles, thus minimizing the negative influence of water to the reaction.[59] As an example, the siliceous zeolite fixed AuPd nanoparticle catalyst AuPd@S-1 exhibited

https://dx.doi.org/10.1021/acscentsci.0c01130
ACS Cent. Sci. 2020, 6, 1685−1697

remarkably higher activity than the supported metal nanoparticles.

DIFFUSION-DEPENDENT SHAPE-SELECTIVE CATALYSIS

The shape-selective feature of metal@zeolite catalysts is not only limited to sieve the molecules larger or smaller than then micropores, but also can be extended to the molecules with different diffusion rates in the micropores (Figure 6III). For example, in the Pd-catalyzed hydrogenation of furfural, an important biomass platform molecule, many products were obtained with uncontrolled selectivity.[60,61] However, when the Pd@S-1 catalyst was used, the furan product was selectively obtained.[60] The mechanism investigation demonstrates that the zeolite micropores hinder the diffusion of various intermediate products, such as furfuryl alcohol, thus to accelerate its deep hydrogenation to form furan, a molecule that easily diffuses through the zeolite micropores. It provided a persuasive example to explain the diffusion-controlled selectivity in the hydrogenation reactions.

STERIC-ADSORPTION DEPENDENT SELECTIVE CATALYSIS

In the zeolite catalyzed reactions, steric adsorption of molecules in the zeolite micropores could change the reaction routes. This feature is also extended to the metal catalyzed reactions by the metal@zeolite catalysts, where the zeolite micropores control the steric adsorption of molecule on the metal surface, thus optimizing the reactions (Figure 6IV). For example, the 4-nitrochlorobenzene is usually parallel to the Pd surface as it is adsorbed on the commercial Pd/C catalyst, where both the -Cl and -NO_2 groups interact with the Pd sites.[103] However, Pd@Beta exhibited different steric adsorptions of 4-nitrochlorobenzene, which is nearly vertical to the Pd surface with the -NO_2 group interacting with Pd.[103] Such adsorption is due to the confinement effect of zeolite micropores, which geometrically modulates the molecular steric adsorption on the Pd surface and in the micropores. The unique adsorption behavior of 4-nitrochlorobenzene on Pd@Beta led to selective hydrogenation of -NO_2 groups with >99% selectivity to the 4-chloroaniline, while the Pd/C could catalyze the hydrogenation of both groups to give aniline as a byproduct.

HYDROGEN SPILLOVER-DEPENDENT SELECTIVE CATALYSIS

The zeolite micropores could effectively adjust the hydrogen spillover, a crucial factor for the hydrogenation reactions (Figure 6V).[109−112] For example, the zeolite microporous environment of Rh@MFI zeolite strongly influences the catalyzed CO_2 hydrogenation.[113] The Rh nanoparticles in proton-form ZSM-5 zeolite (Rh@HZSM-5) exhibits methanation as a dominant reaction, while the K-form zeolite catalyst (Rh@HZSM-5) shows CO selectivity higher than that of methane. In contrast, the siliceous S-1 zeolite fixed Rh (Rh@S-1) exhibited a reverse water−gas shift as a dominant reaction. If the silanol groups were induced into the siliceous zeolite, the CO selectivity was obviously decreased, giving more methane in the products. By using the WO_3 as a probing agent, the hydrogen spillover ability of different catalysts was identified, following the order of S-1 < KZSM-5 < S-1-OH < HZSM-5 in Rh@zeolite catalysts, which is in good agreement with the selectivity trend on these catalysts, where stronger hydrogen spillover ability caused more methane products. This phenomenon is very consistent with the general knowledge, where the hydrogen spillover leads to the formation of highly active hydrogen species that favor the deep hydrogenation of CO/CO_2 into methane, thus giving different product selectivities on the Rh@zeolite catalysts. The protons and H of Si−OH in the zeolite micropores act as carriers for hydrogen spillover, while the general siliceous micropores and the micropores with K^+ species minimized the hydrogen spillover.[113] In addition, it was found that S-1 zeolite micropores also weaken the CO adsorption, which accelerates the rapid CO desorption from the Rh surface that also contributes to the hindered deep hydrogenation.

The advantages of the metal@zeolite structure are obviously observed in RhMn catalyzed syngas transformation, where RhMn@S-1 (RhMn nanoparticles fixed in S-1 zeolite) exhibited a 9-fold higher ethanol productivity than the supported RhMn nanoparticles catalysts.[114] Several reasons were identified for the unusual catalytic performances: the hindered hydrogen spillover in the siliceous zeolite, as discussed above, could hinder deep hydrogenation and contribute to the oxygenate production; the well-defined Rh-MnO_x interfacial nanostructure is highly stable under the reaction conditions, thus maintaining the abundant active sites for oxygenate formation; the confinement effect of zeolite micropores weakens the intermediate adsorption and reduces the energy barriers for C−C coupling.

OUTLOOK

Overall, we briefly summarized synthetic strategies to design metal@zeolite materials with controllable metal and zeolite structures, including single-site metal and small clusters in zeolite micropores, and the industrial-diameter metal nanoparticles fixed in zeolite crystals. A series of metal@zeolite materials not only act as persuasive models for understanding the structure−performance relationships but also provide promising catalysts for the practical utilization. The superior sinter resistance of metal nanoparticles in zeolite crystals would accelerate the development of new catalysts with superior durability, which could reduce the industrial cost particularly for the catalysts containing noble metals. The synergism between metal nanoparticles and zeolite micropores would improve the efficacy of current reactions, and even promote new reaction processes in the future.

Yet, it is still challenging to synthesize metal@zeolite materials with high metal content. The visualization and analysis of the microstructure is still challenging, particularly for the location of metal in zeolite. For example, for the metal@MFI materials, the noble metal cations or nanoclusters are localized in the 10-MR ring of MFI structure, but there are still some opinions that they are in the 5- or 6-MR. The accurate identification of the metal location and the metal-zeolite interface structure requires combining the multiple advanced characterization techniques including electronic tomographic microscopy,[17,85,90,115−117] two-dimensional solid-state NMR spectroscopy,[118] as well as the *in situ* spectroscopic characterizations such as Raman and IR with well-designed atmosphere.[119]

We firmly believe that this research area will continue to develop rapidly in the near future, focusing on both synthesis and catalysis. Although solvent-free and organic template/ligand-free methodologies have been developed, they still need

https://dx.doi.org/10.1021/acscentsci.0c01130
ACS Cent. Sci. 2020, 6, 1685−1697

The metal@zeolite structure is anticipated to bring new opportunities for heterogeneous catalysts with unexpected properties.

improvement for potential large-scale production. More importantly, searching more routes to meet the demands of green and low-cost synthesis is always an endless story in catalyst preparation. In addition, most of the current studies in catalysis over the metal@zeolite materials are focused on several model reactions, which requires extending them in the important industrial reactions, particularly for the transformation of carbon resource small molecules (e.g., CO, CO_2, CH_4, C_3H_8), which require the metal active sites and zeolite shape selectivity. As well, the heteroatom zeolite fixed/encapsulated metal nanostructures might be valuable for investigation of catalysis because of the expected synergism between the metal nanostructures and heteroatoms (e.g., their electronic interaction, the tandem catalysis on different active sites) (Figure 6VI). In addition, the heteroatoms might leach from the zeolite framework to alloy with the metal species, forming new active species to boost the catalysis.[120] As well, the adjustable cations in the zeolite micropores provide an opportunity to electronically modulate the metal species to improve the activity.[85,121] Moreover, the new functions of zeolite combining with the metal nanoparticles would lead to new catalysts. A recent example is the molecular-fence effect of hydrophobic zeolite for AuPd nanoparticles, where the zeolite enriched the *in situ* formed H_2O_2 around the metal sites to strengthen the methane oxidation (Figure 6VII).[122] Another new direction for the future metal@zeolite investigation requires combining machine learning and big data,[123] which would guide the design of metal@zeolite materials with multiple functions and desired catalytic properties for specific reactions. Considering the influx of new ideas, development of the characterization and computational techniques, and the great potentiality for wide utilization, metal@zeolite materials should bring new opportunities for heterogeneous catalysts with integrated advantages of metal nanostructures and zeolite matrix, achieving the effect of 1 + 1 is greater than 2.

AUTHOR INFORMATION

Corresponding Authors

Liang Wang − *Key Lab of Biomass Chemical Engineering of Ministry of Education, College of Chemical and Biological Engineering, Zhejiang University, Hangzhou 310027, China;* orcid.org/0000-0002-5826-1866; Email: liangwang@zju.edu.cn

Feng-Shou Xiao − *Key Lab of Biomass Chemical Engineering of Ministry of Education, College of Chemical and Biological Engineering and Key Laboratory of Applied Chemistry of Zhejiang Province, Department of Chemistry, Zhejiang University, Hangzhou 310027, China;* orcid.org/0000-0001-9744-3067; Email: fsxiao@zju.edu.cn

Author

Hai Wang − *Key Lab of Biomass Chemical Engineering of Ministry of Education, College of Chemical and Biological Engineering, Zhejiang University, Hangzhou 310027, China*

Complete contact information is available at: https://pubs.acs.org/10.1021/acscentsci.0c01130

Notes

The authors declare no competing financial interest.

ACKNOWLEDGMENTS

This work is supported by the National Key Research and Development Program of China (2018YFB0604801), National Natural Science Foundation of China (21822203 and 91634201), Natural Science Foundation of Zhejiang Province (LR18B030002), and the fund from Central University (2019XZZX004-02).

REFERENCES

(1) van Deelen, T. W.; Mejía, C. H.; de Jong, K. P. Control of Metal-Support Interactions in Heterogeneous Catalysts to Enhance Activity and Selectivity. *Nat. Catal.* **2019**, *2*, 955−970.

(2) Otor, H. O.; Steiner, J. B.; García-Sancho, C.; Alba-Rubio, A. C. Encapsulation Methods for Control of Catalyst Deactivation: A Review. *ACS Catal.* **2020**, *10*, 7630−7656.

(3) Wang, A.; Li, J.; Zhang, T. Heterogeneous Single-Atom Catalysis. *Nat. Rev. Chem.* **2018**, *2*, 65−81.

(4) Parastaev, A.; Muravev, V.; Osta, E. H.; van Hoof, A. J. F.; Kimpel, T. F.; Kosinov, N.; Hensen, E. J. M. Boosting CO_2 Hydrogenation via Size-Dependent Metal-Support Interactions in Cobalt/Ceria-Based Catalysts. *Nat. Catal.* **2020**, *3*, 526−533.

(5) Matsubu, J. C.; Yang, V. N.; Christopher, P. Isolated Metal Active Site Concentration and Stability Control Catalytic CO_2 Reduction Selectivity. *J. Am. Chem. Soc.* **2015**, *137*, 3076−3084.

(6) Zhang, J.; Wang, H.; Wang, L.; Ali, S.; Wang, C.; Wang, L.; Meng, X.; Li, B.; Su, D. S.; Xiao, F.-S. Wet-Chemistry Strong Metal-Support Interactions in Titania Supported Au Catalysts. *J. Am. Chem. Soc.* **2019**, *141*, 2975−2983.

(7) Cargnello, M.; Delgado Jaén, J. J.; Hernández Garrido, J. C.; Bakhmutsky, K.; Montini, T.; Calvino Gámez, J. J.; Gorte, R. J.; Fornasier, P. Exceptional Activity for Methane Combustion over Modular Pd@CeO_2 Subunits on Functionalized Al_2O_3. *Science* **2012**, *337*, 713−717.

(8) Zhai, Y.; Pierre, D.; Si, R.; Deng, W.; Ferrin, P.; Nilekar, A. U.; Peng, G.; Herron, J. A.; Bell, D. C.; Saltsburg, H.; Mavrikakis, M.; Flytzani-Stephanopoulos, M. Alkali-Stabilized Pt-OH_x Species Catalyze Low-Temperature Water-Gas Shift Reactions. *Science* **2010**, *329*, 1633−1636.

(9) Chen, G.; Zhao, Y.; Fu, G.; Duchesne, P. N.; Gu, L.; Zheng, Y.; Weng, X.; Chen, M.; Zhang, P.; Pao, C.-W.; Lee, J.-F.; Zheng, N. Interfacial Effects in Iron-Nickel Hydroxide-Platinum Nanoparticles Enhance Catalytic Oxidation. *Science* **2014**, *344*, 495−499.

(10) Graciani, J.; Mudiyanselage, K.; Xu, F.; Baber, A. E.; Evans, J.; Senanayake, S. D.; Stacchiola, D. J.; Liu, P.; Hrbek, J.; Sanz, J. F.; Rodriguez, J. A. Highly Active Copper-Ceria and Copper-Ceria-Titania Catalysts for Methanol Synthesis from CO_2. *Science* **2014**, *345*, 546−550.

(11) Niu, Y.; Huang, X.; Wang, Y.; Xu, M.; Chen, J.; Xu, S.; Willinger, M.-G.; Zhang, W.; Wei, M.; Zhang, B. Manipulating Interstitial Carbon Atoms in the Nickel Octahedral Site for Highly Efficient Hydrogenation of Alkyne. *Nat. Commun.* **2020**, *11*, 3324.

(12) Cao, L.; Liu, W.; Luo, Q.; Yin, r.; Wang, B.; Weissenrieder, J.; Soldemo, M.; Yan, H.; Lin, Y.; Sun, Z.; Ma, C.; Zhang, W.; Chen, S.; Wang, H.; Guan, Q.; Yao, t.; Wei, S.; Yang, J.; Lu, J. Atomically Dispersed Iron Hydroxide Anchored on Pt for Preferential Oxidation of CO in H_2. *Nature* **2019**, *565*, 631−635.

(13) Matsubu, J. C.; Zhang, S.; DeRita, L.; Marinkovic, N. S.; Chen, J. G.; Graham, G. W.; Pan, X.; Christopher, P. Adsorbate-Mediated Strong Metal-Support Interactions in Oxide-Supported Rh Catalysts. *Nat. Chem.* **2017**, *9*, 120−127.

(14) Chen, W.; Pan, X.; Bao, X. Tuning of Redox Properties of Iron and Iron Oxides via Encapsulation within Carbon Nanotubes. *J. Am. Chem. Soc.* **2007**, *129*, 7421−7426.

(15) Pan, X.; Bao, X. The Effects of Confinement inside Carbon Nanotubes on Catalysis. *Acc. Chem. Res.* **2011**, *44* (8), 553−562.

(16) Castillejos, E.; Debouttière, P.-J.; Roiban, L.; Solhy, A.; Martinez, V.; Kihn, Y.; Ersen, O.; Philippot, K.; Chaudret, B.; Serp, P. An Efficient Strategy to Drive Nanoparticles into Carbon Nanotubes and the Remarkable Effect of Confinement on Their Catalytic Performance. *Angew. Chem., Int. Ed.* **2009**, *48*, 2529−2533.
(17) Liu, L.; Lopez-Haro, M.; Lopes, C. W.; Rojas-Buzo, S.; Concepcion, P.; Manzorro, R.; Simonelli, L.; Sattler, A.; Serna, P.; Calvino, J. J.; Corma, A. Structural Modulation and Direct Measurement of Subnanometric Bimetallic PtSn Clusters Confined in Zeolites. *Nat. Catal.* **2020**, *3*, 628−638.
(18) Friedrich, H.; Sietsma, J. R. A.; de Jongh, P. E.; Verkleij, A. J.; de Jong, K. P. Measuring Location, Size, Distribution, and Loading of NiO Crystallites in Individual SBA-15 Pores by Electron Tomography. *J. Am. Chem. Soc.* **2007**, *129*, 10249−10254.
(19) Joo, S. H.; Park, J. Y.; Tsung, C.-K.; Yamada, Y.; Yang, P.; Somorjai, G. A. Thermally Stable Pt/Mesoporous Silica Core-Shell Nanocatalysts for High-Temperature Reactions. *Nat. Mater.* **2009**, *8*, 126−131.
(20) Jiang, H.-L.; Akita, T.; Ishida, T.; Haruta, M.; Xu, Q. Synergistic Catalysis of Au@Ag Core-Shell Nanoparticles Stabilized on Metal-Organic Framework. *J. Am. Chem. Soc.* **2011**, *133*, 1304−1306.
(21) Wang, C.; de Krafft, K. E.; Lin, W. Pt Nanoparticles@ Photoactive Metal-Organic Frameworks: Efficient Hydrogen Evolution via Synergistic Photoexcitation and Electron Injection. *J. Am. Chem. Soc.* **2012**, *134*, 7211−7214.
(22) Pan, X.; Fan, Z.; Chen, W.; Ding, Y.; Luo, H.; Bao, X. Enhanced Ethanol Production Inside Carbon-Nanotube Reactors Containing Catalytic Particles. *Nat. Mater.* **2007**, *6*, 507−511.
(23) Wang, D.; Yang, G.; Ma, Q.; Wu, M.; Tan, Y.; Yoneyama, Y.; Tsubaki, N. Confinement Effect of Carbon Nanotubes: Copper Nanoparticles Filled Carbon Nanotubes for Hydrogenation of Methyl Acetate. *ACS Catal.* **2012**, *2*, 1958−1966.
(24) Feyen, M.; Weidenthaler, C.; Güttel, R.; Schlichte, K.; Holle, U.; Lu, A.-H.; Schüth, F. High-Temperature Stable, Iron-Based Core-Shell Catalysts for Ammonia Decomposition. *Chem. - Eur. J.* **2011**, *17*, 598−605.
(25) Zeng, B.; Hou, B.; Jia, L.; Wang, J.; Chen, C.; Sun, Y.; Li, D. Studies of Cobalt Particle Size Effects on Fischer−Tropsch Synthesis over Core-Shell-Structured Catalysts. *ChemCatChem* **2013**, *5*, 3794−3801.
(26) Cundy, C. S.; Cox, P. A. The Hydrothermal Synthesis of Zeolites: History and Development from the Earliest Days to the Present Time. *Chem. Rev.* **2003**, *103*, 663−701.
(27) Choi, M.; Cho, H. S.; Srivastava, R.; Venkatesan, C.; Choi, D.-H.; Ryoo, R. Amphiphilic Organosilane-Directed Synthesis of Crystalline Zeolite with Tunable Mesoporosity. *Nat. Mater.* **2006**, *5*, 718−723.
(28) Farneth, W. E.; Gorte, R. J. Methods for Characterizing Zeolite Acidity. *Chem. Rev.* **1995**, *95*, 615−635.
(29) Choi, M.; Na, K.; Kim, J.; Sakamoto, Y.; Terasaki, O.; Ryoo, R. Stable Single-Unit-Cell Nanosheets of Zeolite MFI as Active and Long-Lived Catalysts. *Nature* **2009**, *461*, 246−249.
(30) Kang, J.; Cheng, K.; Zhang, L.; Zhang, Q.; Ding, J.; Hua, W.; Lou, Y.; Zhai, Q.; Wang, Y. Mesoporous Zeolite-Supported Ruthenium Nanoparticles as Highly Selective Fischer−Tropsch Catalysts for the Production of C5-C11 Isoparaffins. *Angew. Chem., Int. Ed.* **2011**, *50*, 5200−5203.
(31) Cheng, K.; Zhang, L.; Kang, J.; Peng, X.; Zhang, Q.; Wang, Y. Selective Transformation of Syngas into Gasoline-Range Hydrocarbons over Mesoporous H-ZSM-5-Supported Cobalt Nanoparticles. *Chem. - Eur. J.* **2015**, *21*, 1928−1937.
(32) Peng, X.; Cheng, K.; Kang, J.; Gu, B.; Yu, X.; Zhang, Q.; Wang, Y. Impact of Hydrogenolysis on the Selectivity of the Fischer−Tropsch Synthesis: Diesel Fuel Production over Mesoporous Zeolite-Y-Supported Cobalt Nanoparticles. *Angew. Chem., Int. Ed.* **2015**, *54*, 4553−4556.
(33) Wang, L.; Zhang, J.; Yi, X.; Zheng, A.; Deng, F.; Chen, C.; Ji, Y.; Liu, F.; Meng, X.; Xiao, F.-S. Mesoporous ZSM-5 Zeolite-Supported Ru Nanoparticles as Highly Efficient Catalysts for Upgrading Phenolic Biomolecules. *ACS Catal.* **2015**, *5*, 2727−2734.
(34) Zhao, C.; Lercher, J. A. Upgrading Pyrolysis Oil over Ni/HZSM-5 by Cascade Reactions. *Angew. Chem., Int. Ed.* **2012**, *51*, 5935−5940.
(35) Yuan, W.; Zhang, D.; Ou, Y.; Fang, K.; Zhu, B.; Yang, H.; Hansen, T. W.; Wagner, J. B.; Zhang, Z.; Gao, Y.; Wang, Y. Direct In Situ TEM Visualization and Insight into the Facet-Dependent Sintering Behaviors of Gold on TiO_2. *Angew. Chem., Int. Ed.* **2018**, *57*, 16827−16831.
(36) Lu, J.; Fu, B.; Kung, M. C.; Xiao, G.; Elam, J. W.; Kung, H. H.; Stair, P. C. Coking- and Sintering-Resistant Palladium Catalysts Achieved Through Atomic Layer Deposition. *Science* **2012**, *335*, 1205−1208.
(37) Prieto, G.; Zecevic, J.; Friedrich, H.; de Jong, K. P.; de Jongh, P. E. Towards Stable Catalysts by Controlling Collective Properties of Supported Metal Nanoparticles. *Nat. Mater.* **2013**, *12*, 34−39.
(38) Wang, L.; Xu, S.; He, S.; Xiao, F.-S. Rational Construction of Metal Nanoparticles Fixed in Zeolite Crystals as Highly Efficient Heterogeneous Catalysts. *Nano Today* **2018**, *20*, 74−83.
(39) Choi, M.; Wu, Z.; Iglesia, E. Mercaptosilane-Assisted Synthesis of Metal Clusters within Zeolites and Catalytic Consequences of Encapsulation. *J. Am. Chem. Soc.* **2010**, *132*, 9129−9137.
(40) Goel, S.; Zones, S. I.; Iglesia, E. Encapsulation of Metal Clusters within MFI via Interzeolite Transformations and Direct Hydrothermal Syntheses and Catalytic Consequences of Their Confinement. *J. Am. Chem. Soc.* **2014**, *136*, 15280−15290.
(41) Yan, Y.; Zhang, Z.; Bak, S.-M.; Yao, S.; Hu, X.; Shadike, Z.; Do-Thanh, C.-L.; Zhang, F.; Chen, H.; Lyu, X.; Chen, K.; Zhu, Y.; Lu, X.; Ouyang, P.; Fu, J.; Dai, S. Confinement of Ultrasmall Cobalt Oxide Clusters within Silicalite-1 Crystals for Efficient Conversion of Fructose into Methyl Lactate. *ACS Catal.* **2019**, *9*, 1923−1930.
(42) Laursen, A. B.; Højholt, K. T.; Lundegaard, L. F.; Simonsen, S. B.; Helveg, S.; Schüth, F.; Paul, M.; Grunwaldt, J.-D.; Kegnæs, S.; Christensen, C. H.; Egeblad, K. Substrate Size-Selective Catalysis with Zeolite-Encapsulated Gold Nanoparticles. *Angew. Chem., Int. Ed.* **2010**, *49*, 3504−3507.
(43) Gu, J.; Zhang, Z.; Hu, P.; Ding, L.; Xue, N.; Peng, L.; Guo, X.; Lin, M.; Ding, W. Platinum Nanoparticles Encapsulated in MFI Zeolite Crystals by a Two-Step Dry Gel Conversion Method as a Highly Selective Hydrogenation Catalyst. *ACS Catal.* **2015**, *5*, 6893−6901.
(44) Li, Y. J.; Battavio, P. J.; Armor, J. N. Effect of Water Vapor on the Selective Reduction of NO by Methane over Cobalt-Exchanged ZSM-5. *J. Catal.* **1993**, *142*, 561−571.
(45) Zhao, Z.; Yu, R.; Zhao, R.; Shi, C.; Gies, H.; Xiao, F.-S.; De Vos, D.; Yokoi, T.; Bao, X.; Kolb, U.; Feyen, M.; McGuire, R.; Maurer, S.; Moini, A.; Muller, U.; Zhang, W. Cu-Exchanged Al-Rich SSZ-13 Zeolite from Organotemplate-Free Synthesis as NH_3-SCR Catalyst: Effects of Na^+ Ions on the Activity and Hydrothermal Stability. *Appl. Catal., B* **2017**, *217*, 421−428.
(46) Sushkevich, V. L.; Palagin, D.; Ranocchiari, M.; van Bokhoven, J. A. Selective Anaerobic Oxidation of Methane Enables Direct Synthesis of Methanol. *Science* **2017**, *356*, 523−527.
(47) Maeno, Z.; Yasumura, S.; Wu, X.; Huang, M.; Liu, C.; Toyao, T.; Shimizu, K.-i. Isolated Indium Hydrides in CHA Zeolites: Speciation and Catalysis for Nonoxidative Dehydrogenation of Ethane. *J. Am. Chem. Soc.* **2020**, *142*, 4820−4832.
(48) Gao, J.; Zheng, Y.; Jehng, J.-M.; Tang, Y.; Wachs, I. E.; Podkolzin, S. G. Identification of Molybdenum Oxide Nanostructures on Zeolites for Natural Gas Conversion. *Science* **2015**, *348*, 686−690.
(49) Xiao, F.-S.; Zheng, S.; Sun, J.; Yu, R.; Qiu, S.; Xu, R. Dispersion of Inorganic Salts into Zeolites and Their Pore Modification. *J. Catal.* **1998**, *176*, 474−487.
(50) Zhan, B.-Z.; White, M. A.; Sham, T.-K.; Pincock, J. A.; Doucet, R. J.; Rao, K. V. R.; Robertson, K. N.; Cameron, T. S. Zeolite-Confined Nano-RuO_2: A Green, Selective, and Efficient Catalyst for Aerobic Alcohol Oxidation. *J. Am. Chem. Soc.* **2003**, *125*, 2195−2199.

https://dx.doi.org/10.1021/acscentsci.0c01130
ACS Cent. Sci. 2020, 6, 1685−1697

(51) Chakraborty, S.; Zhang, J.; Krause, J. A.; Guan, H. An Efficient Nickel Catalyst for the Reduction of Carbon Dioxide with a Borane. *J. Am. Chem. Soc.* **2010**, *132*, 8872−8873.
(52) Wang, N.; Sun, Q.; Bai, R.; Li, X.; Guo, G.; Yu, J. In Situ Confinement of Ultrasmall Pd Clusters within Nanosized Silicalite-1 Zeolite for Highly Efficient Catalysis of Hydrogen Generation. *J. Am. Chem. Soc.* **2016**, *138*, 7484−7487.
(53) Yang, H.; Chen, H.; Chen, J.; Omotoso, O.; Ring, Z. Shape Selective and Hydrogen Spillover Approach in the Design of Sulfur-Tolerant Hydrogenation Catalysts. *J. Catal.* **2006**, *243*, 36−42.
(54) Yu, W.-Y.; Zhang, L.; Mullen, G. M.; Henkelman, G.; Mullins, C. B. Oxygen Activation and Reaction on Pd-Au Bimetallic Surfaces. *J. Phys. Chem. C* **2015**, *119*, 11754−11762.
(55) Sun, Q.; Wang, N.; Bing, Q.; Si, R.; Liu, J.; Bai, R.; Zhang, P.; Jia, M.; Yu, J. Subnanometric Hybrid Pd-M(OH)$_2$, M = Ni, Co, Clusters in Zeolites as Highly Efficient Nanocatalysts for Hydrogen Generation. *Chem.* **2017**, *3*, 477−493.
(56) Goel, S.; Wu, Z.; Zones, S. I.; Iglesia, E. Synthesis and Catalytic Properties of Metal Clusters Encapsulated within Small-Pore (SOD, GIS, ANA) Zeolites. *J. Am. Chem. Soc.* **2012**, *134*, 17688−17695.
(57) Sun, Q.; Wang, N.; Zhang, T.; Bai, R.; Mayoral, A.; Zhang, P.; Zhang, Q.; Terasaki, O.; Yu, J. Zeolite-Encaged Single-Atom Rhodium Catalysts: Highly-Efficient Hydrogen Generation and Shape-Selective Tandem Hydrogenation of Nitroarenes. *Angew. Chem., Int. Ed.* **2019**, *58*, 18570−18576.
(58) Sun, Q.; Wang, N.; Fan, Q.; Zeng, L.; Mayoral, A.; Miao, S.; Yang, R.; Jiang, Z.; Zhou, W.; Zhang, J.; Zhang, T.; Xu, J.; Zhang, P.; Cheng, J.; Yang, D.-C.; Jia, R.; Li, L.; Zhang, Q.; Wang, Y.; Terasaki, O.; Yu, J. Subnanometer Bimetallic Pt-Zn Clusters in Zeolites for Propane Dehydrogenation. *Angew. Chem., Int. Ed.* **2020**, DOI: 10.1002/anie.202003349.
(59) Zhang, J.; Wang, L.; Zhu, L.; Wu, Q.; Chen, C.; Wang, X.; Ji, Y.; Meng, X.; Xiao, F.-S. Solvent-Free Synthesis of Zeolite Crystals Encapsulating Gold-Palladium Nanoparticles for the Selective Oxidation of Bioethanol. *ChemSusChem* **2015**, *8*, 2867−2871.
(60) Wang, C.; Wang, L.; Zhang, J.; Wang, H.; Lewis, J. P.; Xiao, F.-S. Product Selectivity Controlled by Zeolite Crystals in Biomass Hydrogenation over a Palladium Catalyst. *J. Am. Chem. Soc.* **2016**, *138*, 7880−7883.
(61) Wang, C.; Liu, Z.; Wang, L.; Dong, X.; Zhang, J.; Wang, G.; Han, S.; Meng, X.; Zheng, A.; Xiao, F.-S. Importance of Zeolite Wettability for Selective Hydrogenation of Furfural over Pd@Zeolite Catalysts. *ACS Catal.* **2018**, *8*, 474−481.
(62) Zhang, J.; Wang, L.; Zhang, B.; Zhao, H.; Kolb, U.; Zhu, Y.; Liu, L.; Han, Y.; Wang, G.; Wang, C.; Su, D. S.; Gates, B. C.; Xiao, F.-S. Sinter-Resistant Metal Nanoparticle Catalysts Achieved by Immobilization Within Zeolite Crystals via Seed-Directed Growth. *Nat. Catal.* **2018**, *1*, 540−546.
(63) Zhu, J.; Osuga, R.; Ishikawa, R.; Shibata, N.; Ikuhara, Y.; Kondo, J. N.; Ogura, M.; Yu, J.; Wakihara, T.; Liu, Z.; Okubo, T. Ultrafast Encapsulation of Metal Nanoclusters into MFI Zeolite in the Course of Its Crystallization: Catalytic Application for Propane Dehydrogenation. *Angew. Chem., Int. Ed.* **2020**, DOI: 10.1002/anie.202007044.
(64) Zhang, Q.; Yu, J.; Corma, A. Applications of Zeolites to C1 Chemistry: Recent Advances, Challenges, and Opportunities. *Adv. Mater.* **2020**,2002927.
(65) Kwak, J. H.; Zhu, H.; Lee, J. H.; Peden, C. H.; Szanyi, J. Two Different Cationic Positions in Cu-SSZ-13? *Chem. Commun.* **2012**, *48*, 4758−4760.
(66) Kwak, J. H.; Tonkyn, R. G.; Kim, D. H.; Szanyi, J.; Peden, C. H. Excellent Activity and Selectivity of Cu-SSZ-13 in the Selective Catalytic Reduction of NO_x with NH_3. *J. Catal.* **2010**, *275*, 187−190.
(67) Martini, A.; Borfecchia, E.; Lomachenko, K. A.; Pankin, I. A.; Negri, C.; Berlier, G.; Beato, P.; Falsig, H.; Bordiga, S.; Lamberti, C. Composition-Driven Cu-Speciation and Reducibility in Cu-CHA Zeolite Catalysts: A Multivariate XAS/FTIR Approach to Complexity. *Chem. Sci.* **2017**, *8*, 6836−6851.
(68) Deka, U.; Juhin, A.; Eilertsen, E. A.; Emerich, H.; Green, M. A.; Korhonen, S. T.; Weckhuysen, B. M.; Beale, A. M. Confirmation of Isolated Cu^{2+} Ions in SSZ-13 Zeolite as Active Sites in NH_3-Selective Catalytic Reduction. *J. Phys. Chem. C* **2012**, *116*, 4809−4818.
(69) Hernández-Maldonado, A. J.; Yang, R. T. Desulfurization of Liquid Fuels by Adsorption via π Complexation with Cu(I)-Y and Ag-Y Zeolites. *Ind. Eng. Chem. Res.* **2003**, *42*, 123−129.
(70) Biscardi, J. A.; Iglesia, E. Structure and Function of Metal Cations in Light Alkane Reactions Catalyzed by Modified H-ZSM5. *Catal. Today* **1996**, *31*, 207−231.
(71) Biscardi, J. A.; Meitzner, G. D.; Iglesia, E. Structure and Density of Active Zn Species in Zn/H-ZSM5 Propane Aromatization Catalysts. *J. Catal.* **1998**, *179*, 192−202.
(72) Barbosa, L. A. M. M.; van Santen, R. A.; Hafner, J. Stability of Zn(II) Cations in Chabazite Studied by Periodical Density Functional Theory. *J. Am. Chem. Soc.* **2001**, *123*, 4530−4540.
(73) Smeets, P. J.; Hadt, R. G.; Woertink, J. S.; Vanelderen, P.; Schoonheydt, R. A.; Sels, B. F.; Solomon, E. I. Oxygen Precursor to the Reactive Intermediate in Methanol Synthesis by Cu-ZSM-5. *J. Am. Chem. Soc.* **2010**, *132*, 14736−14738.
(74) Woertink, J. S.; Smeets, P. J.; Groothaert, M. H.; Vance, M. A.; Sels, B. F.; Schoonheydt, R. A.; Solomon, E. I. A $[Cu_2O]^{2+}$ Core in Cu-ZSM-5, the Active Site in the Oxidation of Methane to Methanol. *Proc. Natl. Acad. Sci. U. S. A.* **2009**, *106*, 18908−18913.
(75) Alayon, E. M. C.; Nachtegaal, M.; Bodi, A.; van Bokhoven, J. A. Reaction Conditions of Methane-to-Methanol Conversion Affect the Structure of Active Copper Sites. *ACS Catal.* **2014**, *4*, 16−22.
(76) Alayon, E. M. C.; Nachtegaal, M.; Kleymenov, E.; van Bokhoven, J. A. Determination of the Electronic and Geometric Structure of Cu Sites during Methane Conversion over Cu-MOR with X-Ray Absorption Spectroscopy. *Microporous Mesoporous Mater.* **2013**, *166*, 131−136.
(77) Grundner, S.; Markovits, M. A. C.; Li, G.; Tromp, M.; Pidko, E. A.; Hensen, E. J. M.; Jentys, A.; Sanchez-Sanchez, M.; Lercher, J. A. Single-Site Trinuclear Copper Oxygen Clusters in Mordenite for Selective Conversion of Methane to Methanol. *Nat. Commun.* **2015**, *6*, 7546.
(78) Wulfers, M. J.; Teketel, S.; Ipek, B.; Lobo, R. F. Conversion of Methane to Methanol on Copper Containing Small-Pore Zeolites and Zeotypes. *Chem. Commun.* **2015**, *51*, 4447−4450.
(79) Yang, B. L.; Lu, S. Q.; Wu, J.; Wang, H. J. Complex Reactions of Hydration and Etherification of Isobutene over La-Modified Beta Molecular Sieve. *Chin. J. Catal.* **2007**, *28*, 73−79.
(80) Kistler, J. D.; Chotigkrai, N.; Xu, P.; Enderle, B.; Praserthdam, P.; Chen, C.-Y.; Browning, N. D.; Gates, B. C. A Single-Site Platinum CO Oxidation Catalyst in Zeolite KLTL: Microscopic and Spectroscopic Determination of the Locations of the Platinum Atoms. *Angew. Chem., Int. Ed.* **2014**, *53*, 8904−8907.
(81) Ortalan, V.; Uzun, A.; Gates, B. C.; Browning, N. D. Direct Imaging of Single Metal Atoms and Clusters in the Pores of Dealuminated HY Zeolite. *Nat. Nanotechnol.* **2010**, *5*, 506−510.
(82) Shan, J.; Li, M.; Allard, L. F.; Lee, S.; Flytzani-Stephanopoulos, M. Mild Oxidation of Methane to Methanol or Acetic Acid on Supported Isolated Rhodium Catalysts. *Nature* **2017**, *551*, 605−608.
(83) Liu, Y.; Li, Z.; Yu, Q.; Chen, Ya.; Chai, Z.; Zhao, G.; Liu, S.; Cheong, W.-C.; Pan, Y.; Zhang, Q.; Gu, L.; Zheng, L.; Wang, Y.; Lu, Y.; Wang, D.; Chen, C.; Peng, Q.; Liu, Y.; Liu, L.; Chen, J.; Li, Y. A General Strategy for Fabricating Isolated Single Metal Atomic Site Catalysts in Y Zeolite. *J. Am. Chem. Soc.* **2019**, *141*, 9305−9311.
(84) Knopsgerrits, P. P.; Devos, D.; Thibaultstarzyk, F.; Jacobs, P. A. Zeolite-encapsulated Mn(II) Complexes as Catalysts for Selective Alkene Oxidation. *Nature* **1994**, *369*, 543−546.
(85) Liu, L.; Lopez-Haro, M.; Lopes, C. W.; Li, C.; Concepcion, P.; Simonelli, L.; Calvino, J. J.; Corma, A. Regioselective Generation and Reactivity Control of Subnanometric Platinum Clusters in Zeolites for High-Temperature Catalysis. *Nat. Mater.* **2019**, *18*, 866−873.
(86) Yang, D.; Xu, P.; Browning, N. D.; Gates, B. C. Tracking Rh Atoms in Zeolite HY: First Steps of Metal Cluster Formation and

https://dx.doi.org/10.1021/acscentsci.0c01130
ACS Cent. Sci. 2020, 6, 1685−1697

Influence of Metal Nucleality on Catalysis of Ethylene Hydrogenation and Ethylene Dimerization. *J. Phys. Chem. Lett.* **2016**, *7*, 2537−2543.
(87) Sun, Q.; Chen, B. W.J.; Wang, N.; He, Q.; Chang, A.; Yang, C.-M.; Asakura, H.; Tanaka, T.; Hülsey, M. J.; Wang, C.-H.; Yu, J.; Yan, N. Zeolite-Encaged Pd-Mn Nanocatalysts for CO_2 Hydrogenation and Formic Acid Dehydrogenation. *Angew. Chem., Int. Ed.* **2020**, DOI: 10.1002/anie.202008962.
(88) Zones, S. I. Conversion of Faujasites to High-Silica Chabazite SSZ-13 in the Presence of *N,N,N*-Trimethyl-1-Adamantammonium Iodide. *J. Chem. Soc., Faraday Trans.* **1991**, *87*, 3709−3716.
(89) Sano, T.; Itakura, M.; Sadakane, M. High Potential of Interzeolite Conversion Method for Zeolite Synthesis. *J. Jpn. Pet. Inst.* **2013**, *56*, 183−197.
(90) Moliner, M.; Gabay, J. E.; Kliewer, C. E.; Carr, R. T.; Guzman, J.; Casty, G. L.; Serna, P.; Corma, A. Reversible Transformation of Pt Nanoparticles into Single Atoms inside High-Silica Chabazite Zeolite. *J. Am. Chem. Soc.* **2016**, *138*, 15743−15750.
(91) Liu, L.; Díaz, U.; Arenal, R.; Agostini, G.; Concepción, P.; Corma, A. Generation of Subnanometric Platinum with High Stability During Transformation of a 2D Zeolite into 3D. *Nat. Mater.* **2017**, *16*, 132−138.
(92) Kurzman, J. A.; Misch, L. M.; Seshadri, R. Chemistry of Precious Metal Oxides Relevant to Heterogeneous Catalysis. *Dalton Trans.* **2013**, *42*, 14653−14667.
(93) Yu-Yao, Y.-F.; Kummer, J. T. Low-Concentration Supported Precious Metal Catalysts Prepared by Thermal Transport. *J. Catal.* **1987**, *106*, 307−312.
(94) Carrillo, C.; Johns, T. R.; Xiong, H.; DeLaRiva, A.; Challa, S. R.; Goeke, R. S.; Artyushkova, K.; Li, W.; Kim, C. H.; Datye, A. K. Trapping of Mobile Pt Species by PdO Nanoparticles under Oxidizing Conditions. *J. Phys. Chem. Lett.* **2014**, *5*, 2089−2093.
(95) Iglesias-Juez, A.; Kubacka, A.; Fernandez-Garcia, M.; Di Michiel, M.; Newton, M. A. Nanoparticulate Pd Supported Catalysts: Size-Dependent Formation of Pd(I)/Pd(0) and Their Role in CO Elimination. *J. Am. Chem. Soc.* **2011**, *133*, 4484−4489.
(96) Xiao, F. S.; Weber, W. A.; Alexeev, O.; Gates, B. C. Probing the Limits of Structure Insensitivity: Size-Dependent Catalytic Activity of Al_2O_3-Supported Iridium Clusters and Particles for Toluene Hydrogenation. *Stud. Surf. Sci. Catal.* **1996**, *101*, 1135−1144.
(97) Xu, Z.; Yue, Y.; Bao, X.; Xie, Z.; Zhu, H. Propane Dehydrogenation over Pt Clusters Localized at the Sn Single-Site in Zeolite Framework. *ACS Catal.* **2020**, *10*, 818−828.
(98) Ding, L.; Shi, T.; Gu, J.; Cui, Y.; Zhang, Z.; Yang, C.; Chen, T.; Lin, M.; Wang, P.; Xue, N.; Peng, L.; Guo, X.; Zhu, Y.; Chen, Z.; Ding, W. CO_2 Hydrogenation to Ethanol over Cu@Na-Beta. *Chem.* **2020**, DOI: 10.1016/j.chempr.2020.07.001.
(99) Wu, Q.; Liu, X.; Zhu, L.; Ding, L.; Gao, P.; Wang, X.; Pan, S.; Bian, C.; Meng, X.; Xu, J.; Deng, F.; Maurer, S.; Müller, U.; Xiao, F.-S. Solvent-Free Synthesis of Zeolites from Anhydrous Starting Raw Solids. *J. Am. Chem. Soc.* **2015**, *137*, 1052−1055.
(100) Ren, L.; Wu, Q.; Yang, C.; Zhu, L.; Li, C.; Zhang, P.; Zhang, H.; Meng, X.; Xiao, F.-S. Solvent-Free Synthesis of Zeolites from Solid Raw Materials. *J. Am. Chem. Soc.* **2012**, *134*, 15173−15176.
(101) Sazama, P.; Moravkova, J.; Sklenak, S.; Vondrova, A.; Tabor, E.; Sadovska, G.; Pilar, R. Effect of the Nuclearity and Coordination of Cu and Fe Sites in Beta Zeolites on the Oxidation of Hydrocarbons. *ACS Catal.* **2020**, *10*, 3984−4002.
(102) Guo, X.; Xu, M.; She, M.; Zhu, Y.; Shi, T.; Chen, Z.; Peng, L.; Guo, X.; Lin, M.; Ding, W. CuO@SAPO-34 and Pore Mouth Catalysis for One-pot Oxidation of Cyclohexane. *Angew. Chem., Int. Ed.* **2020**, *59*, 2606−2611.
(103) Zhang, J.; Wang, L.; Shao, Y.; Wang, Y.; Gates, B. C.; Xiao, F.-S. A Pd@Zeolite Catalyst for Nitroarene Hydrogenation with High Product Selectivity by Sterically Controlled Adsorption in the Zeolite Micropores. *Angew. Chem., Int. Ed.* **2017**, *56*, 9747−9751.
(104) Cui, T.-L.; Ke, W.-Y.; Zhang, W.-B.; Wang, H.-H.; Li, X.-H; Chen, J.-S. Encapsulating Palladium Nanoparticles Inside Mesoporous MFI Zeolite Nanocrystals for Shape-Selective Catalysis. *Angew. Chem., Int. Ed.* **2016**, *55*, 9178−9182.
(105) Christensen, C. H.; Jørgensen, B.; Rass-Hansen, J.; Egeblad, K.; Madsen, R.; Klitgaard, S. K.; Hansen, S. M.; Hansen, M. R.; Andersen, H. C.; Riisager, A. Formation of Acetic Acid by Aqueous-Phase Oxidation of Ethanol with Air in the Presence of a Heterogeneous Gold Catalyst. *Angew. Chem., Int. Ed.* **2006**, *45*, 4648−4651.
(106) Simakova, A.; Sobolev, V. I.; Koltunov, K. Y.; Campo, B.; Leino, A.-R.; Kordás, K.; Murzin, D. Y. Double-Peak" Catalytic Activity of Nanosized Gold Supported on Titania in Gas-Phase Selective Oxidation of Ethanol. *ChemCatChem* **2010**, *2*, 1535−1538.
(107) Mielby, J.; Abildstrøm, J. O.; Wang, F.; Kasama, T.; Weidenthaler, C.; Kegnæs, S. Oxidation of Bioethanol using Zeolite-Encapsulated Gold Nanoparticles. *Angew. Chem., Int. Ed.* **2014**, *53*, 12513−12516.
(108) Jørgensen, B.; Christiansen, S. E.; Thomsen, M. L. D.; Christensen, C. H. Aerobic Oxidation of Aqueous Ethanol Using Heterogeneous Gold Catalysts: Efficient Routes to Acetic Acid and Ethyl Acetate. *J. Catal.* **2007**, *251*, 332−337.
(109) Kyriakou, G.; Boucher, M. B.; Jewell, A. D.; Lewis, E. A.; Lawton, T. J.; Baber, A. E.; Tierney, H. L.; Flytzani-Stephanopoulos, M.; Sykes, E. C. H. Isolated Metal Atom Geometries as a Strategy for Selective Heterogeneous Hydrogenations. *Science* **2012**, *335*, 1209−1212.
(110) Jiang, L.; Liu, K.; Hung, S.-F.; Zhou, L.; Qin, R.; Zhang, Q.; Liu, P.; Gu, L.; Chen, H. M.; Fu, G.; Zheng, N. Facet Engineering Accelerates Spillover Hydrogenation on Highly Diluted Metal Nanocatalysts. *Nat. Nanotechnol.* **2020**, DOI: 10.1038/s41565-020-0746-x.
(111) Marcinkowski, M. D.; Jewell, A. D.; Stamatakis, M.; Boucher, M. B.; Lewis, E. A.; Murphy, C. J.; Kyriakou, G.; Sykes, E. C. H. Controlling a Spillover Pathway with the Molecular Cork Effect. *Nat. Mater.* **2013**, *12*, 523−528.
(112) Wang, S.; Zhao, Z.-J.; Chang, X.; Zhao, J.; Tian, H.; Yang, C.; Li, M.; Fu, Q.; Mu, R.; Gong, J. Activation and Spillover of Hydrogen on Sub-1 nm Palladium Nanoclusters Confined within Sodalite Zeolite for the Semi Hydrogenation of Alkynes. *Angew. Chem., Int. Ed.* **2019**, *58*, 7668−7672.
(113) Wang, C.; Guan, E.; Wang, L.; Chu, X.; Wu, Z.; Zhang, J.; Yang, Z.; Jiang, Y.; Zhang, L.; Meng, X.; Gates, B. C.; Xiao, F.-S. Product Selectivity Controlled by Nanoporous Environments in Zeolite Crystals Enveloping Rhodium Nanoparticle Catalysts for CO_2 Hydrogenation. *J. Am. Chem. Soc.* **2019**, *141*, 8482−8488.
(114) Wang, C.; Zhang, J.; Qin, G.; Wang, L.; Zuidema, E.; Yang, Q.; Dang, S.; Yang, C.; Xiao, J.; Meng, X.; Mesters, C.; Xiao, F.-S. Direct Conversion of Syngas to Ethanol within Zeolite Crystals. *Chem.* **2020**, *6*, 646−657.
(115) Ma, Y.; Oleynikov, P.; Terasaki, O. Electron Crystallography for Determining the Handedness of a Chiral Zeolite Nanocrystal. *Nat. Mater.* **2017**, *16*, 755−759.
(116) Liu, L.; Lopez-Haro, M.; Calvino, J. J.; Corma, A. Tutorial: Structural Characterization of Isolated Metal Atoms and Subnanometric Metal Clusters in Zeolites. *Nat. Protoc.* **2020**, DOI: 10.1038/s41596-020-0366-9.
(117) Liu, L.; Lopez-Haro, M.; Meira, D. M.; Concepcion, P.; Calvino, J. J.; Corma, A. Regioselective Generation of Single-Site Iridium Atoms and Their Evolution into Stabilized Subnanometric Iridium Clusters in MWW Zeolite. *Angew. Chem., Int. Ed.* **2020**, *59*, 15695−15702.
(118) Xu, J.; Wang, Q.; Deng, F. Metal Active Sites and Their Catalytic Functions in Zeolites: Insights from Solid-State NMR Spectroscopy. *Acc. Chem. Res.* **2019**, *52*, 2179−2189.
(119) Chai, Y.; Han, X.; Li, W.; Liu, S.; Yao, S.; Wang, C.; Shi, W.; da-Silva, I.; Manuel, P.; Cheng, Y.; Daemen, L. D.; Ramirez-Cuesta, A. J.; Tang, C. C.; Jiang, L.; Yang, S.; Guan, N.; Li, L. Control of Zeolite Pore Interior for Chemoselective Slkyne/Olefin Deparations. *Science* **2020**, *368*, 1002−1006.
(120) Iida, T.; Zanchet, D.; Ohara, K.; Wakihara, T.; Román-Leshkov, Y. Concerted Bimetallic Nanocluster Synthesis and Encapsulation via Induced Zeolite Framework Demetallation for

Shape and Substrate Selective Heterogeneous Catalysis. *Angew. Chem., Int. Ed.* **2018**, *57*, 6454−6458.
(121) Zhang, Z.; Li, Y.; Gu, J.; Ding, L.; Xue, N.; Peng, L.; Guo, X.; Zhu, Y.; Ma, J.; Ding, W. The Effect of Electrostatic Field on the Catalytic Properties of Platinum Clusters Confined in Zeolite for Hydrogenation. *Catal. Sci. Technol.* **2018**, *8*, 6384−6395.
(122) Jin, Z.; Wang, L.; Zuidema, E.; Mondal, K.; Zhang, M.; Zhang, J.; Wang, C.; Meng, X.; Yang, H.; Mesters, C.; Xiao, F.-S. Hydrophobic Zeolite Modification for in situ Peroxide Formation in Methane Oxidation to Methanol. *Science* **2020**, *367*, 193−197.
(123) Moliner, M.; Román-Leshkov, Y.; Corma, A. Machine Learning Applied to Zeolite Synthesis: The Missing Link for Realizing High-Throughput Discovery. *Acc. Chem. Res.* **2019**, *52*, 2971−2980.

https://dx.doi.org/10.1021/acscentsci.0c01130
ACS Cent. Sci. 2020, 6, 1685−1697